REPORT DOCUMENTATION PAGE

Form Approved
OMB NO. 0704-0188

1. AGENCY USE ONLY (Leave Blank)	2. REPORT DATE November 1998	3. REPORT TYPE AND DATES COVERED Final Report June 1998 - December 1998

4. TITLE AND SUBTITLE
Feasibility Study on Deformation Energy Absorption of Metal Foams at High Strain Rates

5. FUNDING NUMBERS
DAAG55-98-K-0002

6. AUTHOR(S)
C.J. Yu, H.H. Eifert, I.W. Hall, R. Franz, K. Leighton

7. PERFORMING ORGANIZATION NAME(S) AND ADDRESS(ES)
Fraunhofer Resource Center
Newark, DE 19716

8. PERFORMING ORGANIZATION REPORT NUMBER

9. SPONSORING / MONITORING AGENCY NAME(S) AND ADDRESS(ES)
U. S. Army Research Office
P.O. Box 12211
Research Triangle Park, NC 27709-2211

10. SPONSORING / MONITORING AGENCY REPORT NUMBER
ARO 38790.1-MS

11. SUPPLEMENTARY NOTES
The views, opinions and/or findings contained in this report are those of the author(s) and should not be construed as an official Department of the Army position, policy or decision, unless so designated by other documentation.

12 a. DISTRIBUTION / AVAILABILITY STATEMENT
Approved for public release; distribution unlimited.

12 b. DISTRIBUTION CODE

13. ABSTRACT (Maximum 200 words)

Metal foams with a high fraction of porosity have gained their usefulness and are becoming a new class of engineering materials. The property attributes of metal foams include the high specific stiffness (stiffness to weight ratio) and the characteristic non-linear deformation behavior. These attributes lend themselves to the areas where lightweight construction and deformation energy absorption are considered. On the defense-related applications, it may be possible to use metal foam for armor protection for military vehicles and personnel. The shock energy induced by the penetrator can by delayed and absorbed in a tailored, multi-layered armor that includes metal foam.

This project examined the effect of high strain rate on aluminum foams. Split Hopkinson

14. SUBJECT TERMS
metal foams, energy absorption, high strain rates, ballistic impact, armor protection

15. NUMBER OF PAGES

16. PRICE CODE

17. SECURITY CLASSIFICATION OR REPORT	18. SECURITY CLASSIFICATION ON THIS PAGE	19. SECURITY CLASSIFICATION OF ABSTRACT	20. LIMITATION OF ABSTRACT
UNCLASSIFIED	UNCLASSIFIED	UNCLASSIFIED	UL

NSN 7540-01-280-5500

Standard Form 298 (Rev.2-89)
Prescribed by ANSI Std. 239-18
298-102

Pressure Bar test and FSP (Fragment Simulating Projectile) ballistic tests were conducted. Results indicated that compression deformation of the foam is in the form of cell wall buckling and tearing. The ballistic stress wave experiments showed that the metal foam is effective in containing rearward deformation of a ballistic target, and, therefore, may be useful for controlling backface deformation and spalling, thereby providing added protection to equipment and personnel.

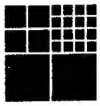

Fraunhofer USA Resource Center
Delaware

Final Report to ARO

Feasibility Study on Deformation Energy Absorption of Metal Foams at High Strain Rates

Section **Page**

List of Figures

List of Figures (Continued)

Page

List of Tables

Acknowledgments

This report is based on work supported by the Army Research Office under Contract No. DAAG55-98-0002. The contributing authors are Dr. Chin-Jye (Mike) Yu, Dr. T. Dennis Claar, and Dr. Harald H. Eifert of the Fraunhofer Resource Center - Delaware, Professor Rick Hall of the University of Delaware, and Mr. Bob Franz and Ms. Kathy Leighton of Lanxide Armor Products, Inc. The authors would like to thank Program Monitors, Dr. John Bailey and Dr. Wilbur Simmons of the Army Research Office, for their valuable support and guidance.

Appreciation is also extended to Mr. Bernie McGuinness for their technical assistance, and Ms. Linda M. Sayther for keeping the accounting straight.

1. INTRODUCTION

Metallic foams with a high fraction of porosity (typical range from 40-98 vol.%) are now becoming a new class of materials for various engineering applications such as filters or heat exchangers for chemical processing and impact energy absorbers in automotive applications. The attributes of metallic foams also lend themselves to other applications when sound and heat isolation, lightweight construction, or energy absorption are considered. The latter two applications make use of the unique characteristics of a metallic cellular material, i.e. the combination of its comparatively high specific strength and its characteristic non-linear deformation behavior [1], and can lead to many unique structural applications.

A powder metallurgy method for fabricating metallic foams was developed at the Fraunhofer Institute for Applied Materials Research (IFAM) [2]. This method allows direct net-shape fabrication of foamed parts with a relatively homogeneous pore structure. Metallic foams fabricated by this approach exhibit closed-cell microstructures with higher mechanical strength compared to the open-cell foams. This type of microstructure is particularly attractive for applications in the field of lightweight construction and energy absorption.

Processing Scheme

The Fraunhofer powder-metallurgy route to produce metallic foams consists of the following steps: (1) mixing of metal powders and suitable foaming agent, (2) compaction or extrusion of powder mixtures; and (3) foaming of pre-compacted, semi-finished part by heating to the melting temperature of metal (Figure 1).

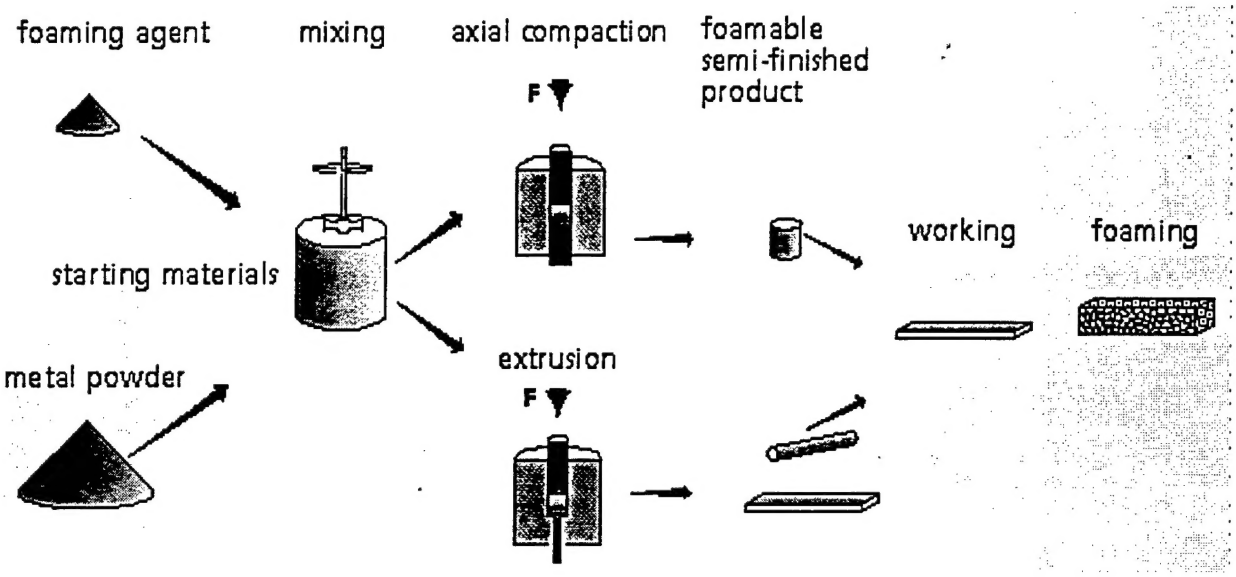

Figure 1: Powder metallurgy route of metal foam production.

Microstructure

Fraunhofer's prior experience in the production of foamed aluminum indicates that the foamed component provides a substantial increase in the stiffness/weight ratio (SWR) with a low fractional density. The aluminum foam has a relatively homogeneous closed-cell microstructure (Figure 2) which is responsible for the high SWR of the foam. Under deformation, this microstructure features localized cell collapse and rapid compaction energy dissipation, which leads to unique deformation behaviors and material properties including high SWR and energy absorption in the material.

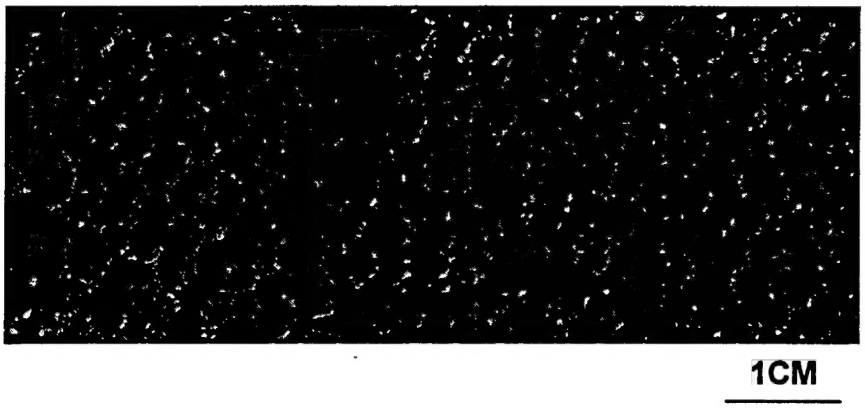

Figure 2: Typical microstructure of aluminum foam.

2. OBJECTIVE

The objective of this feasibility study is to examine the deformation behavior of aluminum foams at high strain rates up to the ballistic range. Currently, the deformation properties of metal foams are evaluated at low strain rates using quasi-static mechanical testing. Very few data are available for foam structures at high strain rates. It is not possible to derive the deformation behavior of metal foams at high strain rate using quasi-static mechanical test results. To better understand the foam material's deformation behavior as a function of strain rate, the following tasks were designed and conducted: (1) fabrication of foam material and design of test target, (2) quasi-static testing and Split Hopkinson Pressure Bar testing (strain rate up to 10^3 s^{-1}), and (3) ballistic testing (strain rate up to 10^5 s^{-1}). The following sections will describe the experimental approaches and test results.

3. EXPERIMENTS

Fabrication of foam materials and design of test target for ballistic testing

For all of the experiments conducted in this project, Al6061 foams with porosities ranging from 70% to 80% were selected and fabricated. These aluminum foams were manufactured by the Fraunhofer Resource Center – Delaware (FRC-DE) using aluminum 6061 alloy powder and TiH_2 as the foaming agent.

Quasi-static testing and Split Hopkinson Pressure Bar testing (strain rate: 10^{-1} to 10^{3} s^{-1})

Four different nominal densities of aluminum 6061 foams were produced for these tests. The foams were fabricated as rectangular plates approximately 13x150x150mm and had the typical closed cell structure as shown in Figure 2. Since some cell size variations occurred throughout the plates, the density of each individual test piece was determined by measuring its outer dimensions and weight immediately prior to testing.

Quasi-static compression tests were conducted using a displacement-controlled Instron testing machine at a strain rate of $1.5x10^{3}$ s^{-1}. High strain rate tests were conducted using a compression-type Split Hopkinson Pressure Bar (SHPB). Figure 3 is a schematic of the testing apparatus. Briefly, in this technique a cylindrical specimen is mounted between two long bars, referred to as the incident and transmitter bars, while a third bar, the striker bar, is used to impact to the end of the incident bar. This impact creates a compressive pulse which travels down the incident bar and into the specimen, which then deforms as it is sandwiched between incident and transmitter bars. The strains measured by strain gages on the incident and transmitter bars are then used to determine strain rate, strain, and stress in the specimen using one-dimensional elastic wave analysis on the bars. Details of the SHPB test technique and the corresponding data analysis are given elsewhere [3].

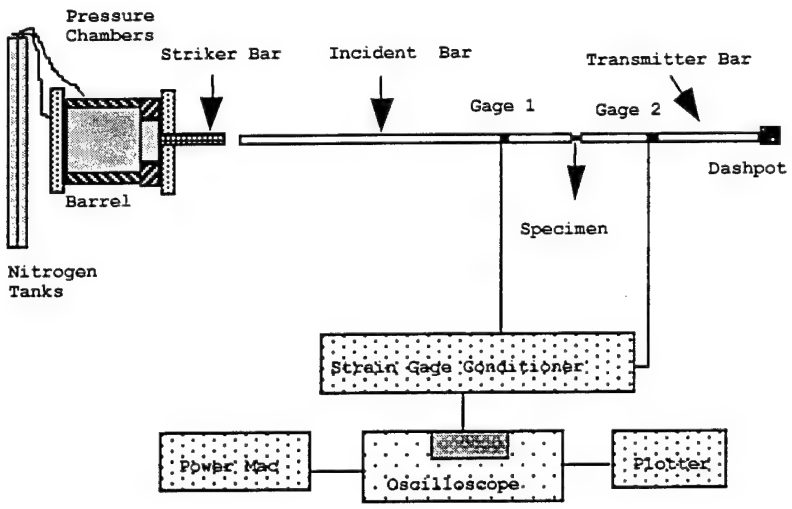

Figure 3: Schematic of Split Hopkinson Pressure Bar testing.

High strain rate tests were conducted on the foams over the range of $3x10^2$ to $2x10^3$ s^{-1}. For the purposes of this initial study, data reduction was carried out the same as for conventional fully dense materials, using the simple 'one wave' analysis. It is recognized that this approach violates several of the underlying assumptions of the analysis since the volume is definitely not constant during deformation and the bars and sample are of vastly different acoustic impedance. Nevertheless, it will be seen that this simple approach yields results which are perfectly compatible with those of quasi-static testing and provide a basis for initial understanding of these materials. Future work should investigate and determine the corrections necessary to ensure entirely dependable values.

In both types of test, cylindrical foam specimens approximately 18 mm in diameter and 12 mm length were compressed. The diameter of the samples was slightly less than that of the bars (19 mm) and, due to the small Poisson's ratio of the foam, specimen diameters during deformation never exceeded the bar diameter within the studied strain levels up to 60% strain. The relatively large diameter of the SHPB used was advantageous, since larger volumes of foam sample could be tested. The top and bottom surfaces of the plates were machined flat and

parallel before specimens were core-drilled from them and weighed in order to calculate density and relative density, ρ^*, before compression testing. The relative density is expressed as:

$$\rho^*=\rho_m/\rho_f \qquad \text{Eqn. 1}$$

where "f" and "m" refer to the foam and precursor metal, respectively. The nominal and relative densities of the four plates tested are given below in Table 1.

Table 1. Densities of Foam Plates Tested

Foam Plate #	Density (g cm^{-3})	Relative Density (%)
1	0.34	12.6
2	0.47	17.4
3	0.57	21.1
4	0.82	30.4

Ballistic testing (strain rate: 10^4 to 10^5 s^{-1})

The goal of the ballistic experiments was to evaluate the use of aluminum foam as a shock energy-absorbing member in ceramic armor systems, and for control of behind-the- target effects such as backface deformation.

A typical configuration for ceramic armor in medium weight military vehicles consists of a metallic cover plate or strike face, bonded to a ceramic tile, subsequently bonded to a metallic backing plate. In this configuration, the ceramic breaks up or deforms the incoming projectile, and the metallic backing "catches" the extant penetrator and ceramic fragments. The metallic cover plate aids the ceramic by providing front face confinement, and may protect the ceramic from field damage.

Upon projectile impact at typical ordnance velocities, a stress wave is generated and propagates through the ceramic. Reflections from boundaries and subsequent stress wave

interactions result in tensile stress states and attendant microcracking. Microcracking due to these impact-induced stress waves weakens the ceramic, allowing the projectile to penetrate more easily. In an armor design utilizing a metal cover plate over the ceramic tile, stress waves from the projectile impact on the metal cover plate can run ahead into the ceramic, and failure may initiate prior to the projectile even contacting the ceramic tile. It is suggested that the aluminum metal foam may be capable of mitigating the impact-induced stress waves and thereby delay damage in the ceramic layers and improve their performance.

The amplitude and frequency of the stress waves produced at impact vary greatly with the nose shape of the projectiles, e.g. ogive vs. cylindrical. The highest amplitude waves have been measured for impacts with fragment simulating projectiles (FSP), which have a chisel, nosed cylindrical shape and are made from mild steel. These projectiles were designed for use in test ranges to simulate artillery fragments, a real battlefield concern.

The ballistic experiments described herein were performed with the 20 mm FSP impacting targets containing layers of aluminum foam, ceramic, and high hardness steel (HHS). The foam layers were expected to adsorb shock energy from the projectile impact and thus delay damage in the ceramic layers and improve their performance. Metal foam layers located behind the ceramic armor strike face were tested as a preliminary investigation into their ability to absorb energy behind a ceramic target.

Ballistic induced stress wave measurement

Piezoresistant stress gages sandwiched in Al2O3 ceramic were used to measure the effect of the foam on stress waves produced by the projectile impact and later time target dynamics. Dynasen Model Mn/Cn 4-50-EK gages were used to measure the stress waves in the experiments. These gages consist of two separate interlaced 50 ohm foil grids enclosed in a polyimide plastic film. One of the grids is made of manganin and is used to measure stress. The other is made of constantan and is used to measure lateral strain. Both grids are 6.35 mm square and 0.127 mm thick. The measured strain is used to correct the stress measurements.

The gages are connected to a Dynasen CK-1-50-300 power supply and bridge circuit, which is triggered upon projectile impact by a "make" screen with a simple capacitor discharge circuit. Signals are recorded on a digital oscilloscope, which is triggered from the power supply.

The data from the two signals obtained from each gage are analyzed using a data reduction and analysis software package [4]. Calibrations are made of each circuit with known dummy gages inserted in the lines instead of the actual gage. Signals from known changes in resistance are then used to determine the circuit constants. These constants along with known bridge and cable resistances are used to calculate the resistance of each grid at each simultaneous time step of the signals. Detailed description of this method can be found in reference 4.

To calculate the stresses in the material surrounding the gages, it is assumed that the resistance of the constantan grid is not affected by the stress field that surrounds both it and the manganin grid. It is further assumed that the strain in the manganin grid is the same as in the constantan grid. Finally it is assumed that the normal stress in the surrounding material is the same as in the manganin.

4. RESULTS AND DISCUSSION

Results of quasi-static testing

Typical quasi-static compression stress-strain curves of the foam are shown for a sample of each density in Figure 4. Clearly, the flow stress of the foam is a strong function of relative density and the stress-strain curve can be divided into three regions, (1) linear elastic region, (2) collapse region (where the compressive stress increases slightly as a function of strain) and (3) densification region (where the compressive stress increases rapidly as a function of strain). In Region 1 the only deformation that occurs is elastic and is due to cell wall bending. This is followed by Region 2, in which the first cell wall buckling event occurs and the stress drops. (Although often referred to as an upper and lower yield stress, this does not correspond to a yield phenomenon in the normal sense.) In Region 3, the foam progressively collapses and densifies. It was observed that deformation in Region 3 was highly localized and proceeded by the advance of a densification front from deformed to undeformed regions of the sample. Since the deformation occurs discontinuously in adjoining cells in Region 2, oscillations in stress were frequently detected due to the repetitive nature of the process of cell collapse and densification. The oscillations were, however, generally superimposed upon a slowly increasing stress.

Figure 5 shows the results of three separate tests on samples of the same nominal density and, not surprisingly, shows first that there is some density variation from sample to sample and second there is some variability even between samples of the same density. The differences would be minimized by the use of larger sized samples. Figures 4 and 5 show that the flow stress (and/or upper yield stress and lower yield stress) increased as the relative density increased while the densification strain decreased as relative density increased.

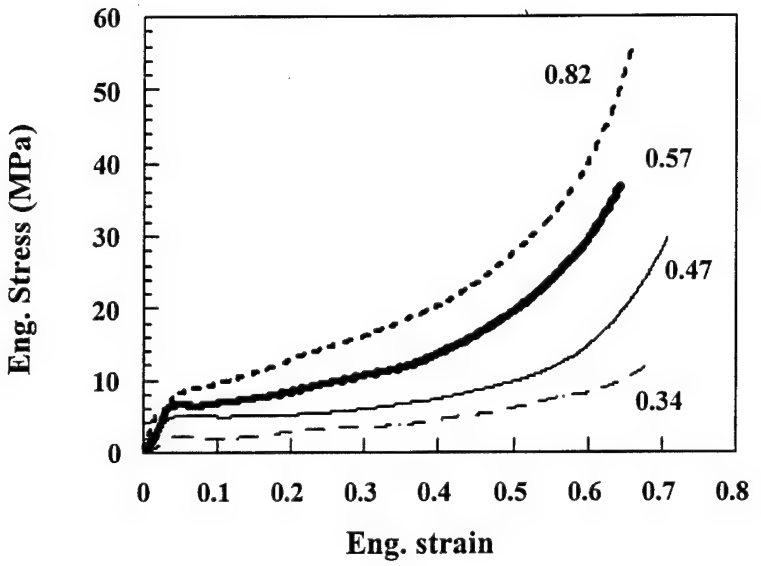

Figure 4: Quasi-static stress *vs.* strain curves for representative samples of each density.

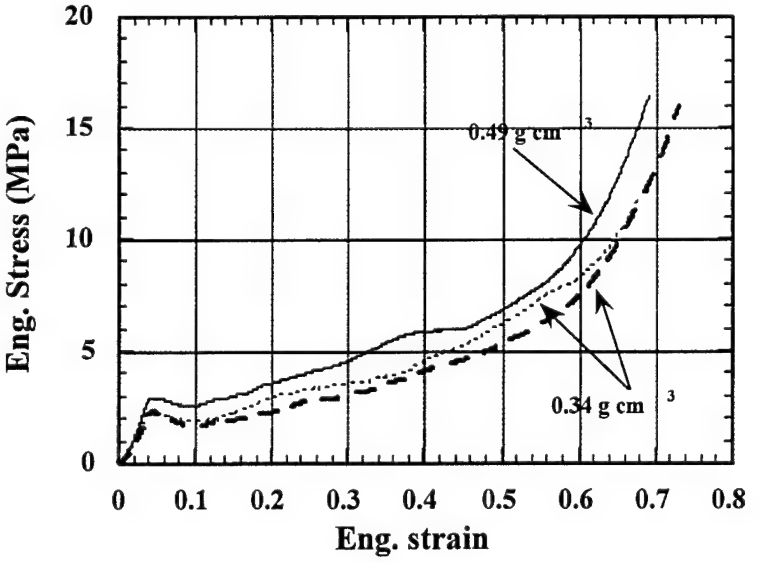

Fig. 5: Quasi-static stress *vs.* strain curves for 3 samples of same nominal density (from plate 1).

Results of Split Hopkinson Bar testing

Similar to quasi-static testing, foam samples of different relative densities were compressed in the SHPB apparatus. Figure 6 presents typical stress-strain curves for 0.34gcm^{-3} foam samples at ~1.9x10^{3} s^{-1} showing the considerable stress drop which occurs at the so-called yield point. Similar data are shown for nominal densities of 0.57 and 0.82 gcm^{-3} in Figures 7 and 8.

It will be noted that the stress *vs.* strain curves presented above from high strain rate tests terminate at strains of approximately 25%. This is an artifact of the SHPB technique, which applies the stress (and, hence, strain) during a short time window before the elastic waves are reflected in the incident bar. Nevertheless it is possible to "construct" stress *vs.* strain curves to higher strains by recording the second, third, fourth etc, reflections in the incident bar and reducing the data accordingly. Figure 9 presents typical raw data from an SHPB experiment that shows the data for the first and second compressive waves. This figure shows (in voltage) the measurements from strain gages on the incident and transmitter bars from which the magnitudes of the incident, reflected and transmitted waves are calculated and from which the stress strain curves are derived.

Figure 10 shows the flow stress at 10% strain plotted *vs.* density for *all the samples tested at all strain rates*. It is readily seen that although there is a spread of data, the flow stress correlated quite well with the density and can be plotted to a power law relationship of the form:

$$\text{Flow stress} = 23.5 \times \rho^{2.2} \text{ MPa, Correlation coefficient (R)} = 0.965 \qquad \text{Eqn. 2}$$

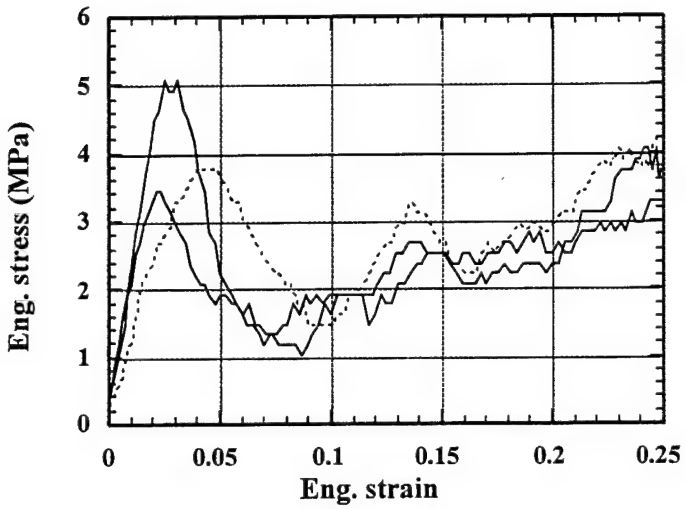

Fig. 6: Stress *vs.* strain curves for 3 samples of nominal density 0.34 gcm^{-3} tested at 1.9x10^{3} s^{-1}.

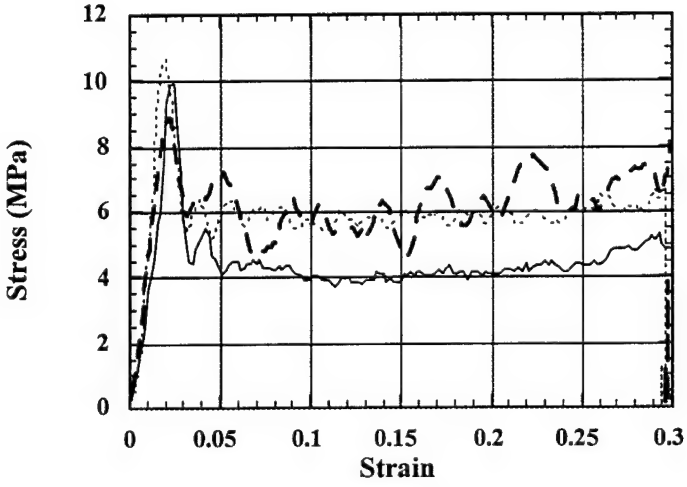

Fig. 7: Stress *vs.* strain curves for 3 samples of nominal density 0.57 gcm^{-3} tested at ~1000 s^{-1}.

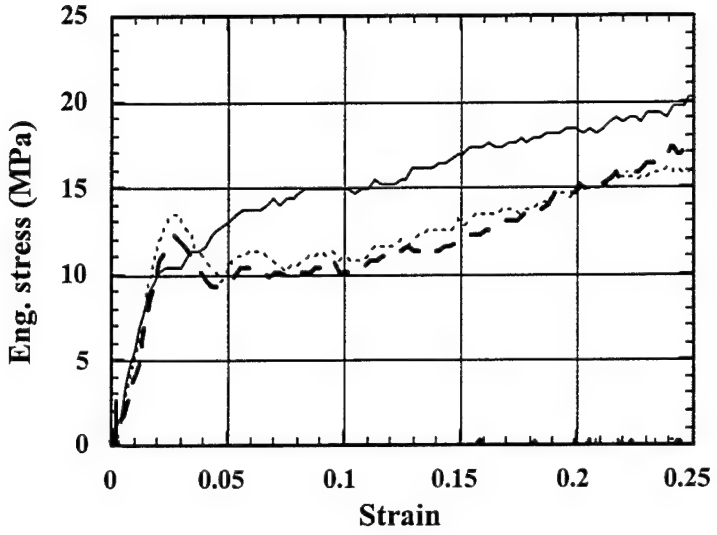

Fig. 8: Stress *vs.* strain curves for 3 samples of nominal density 0.82 gcm^{-3} tested at $1.9x10^3\ s^{-1}$.

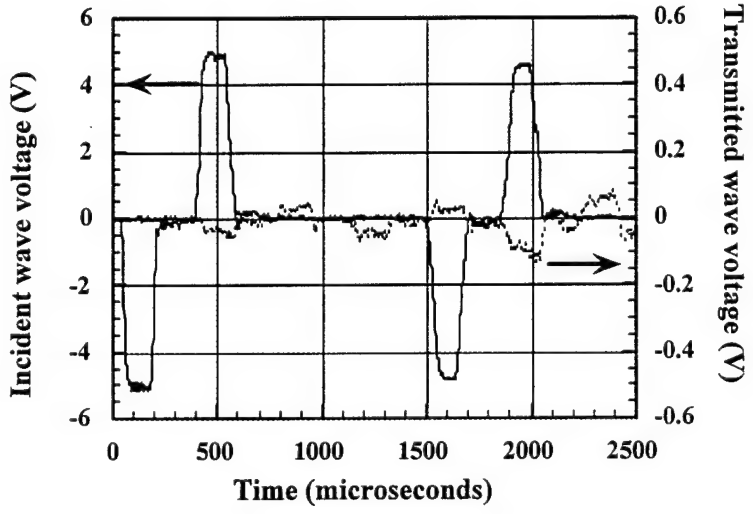

Fig. 9(a): Voltage *vs.* time record for sample showing 2 reflections and stress/strain events.

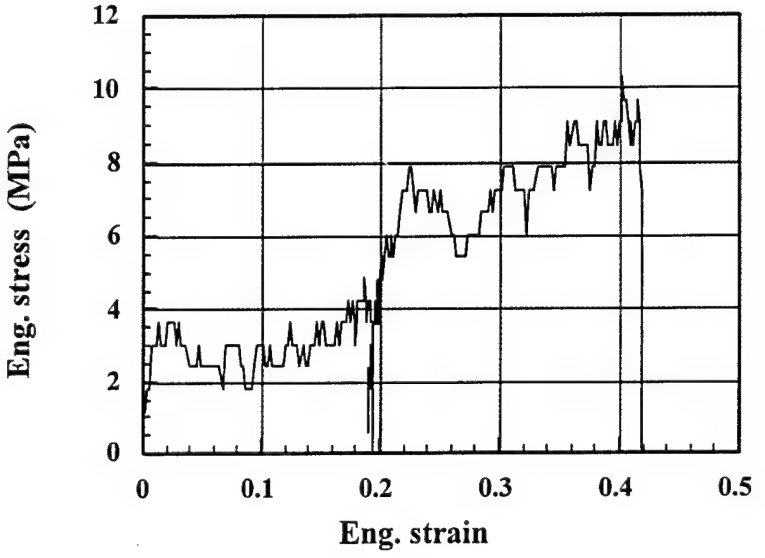

Fig. 9(b): Multi-part stress vs. strain curve constructed from data of Fig. 9(a).

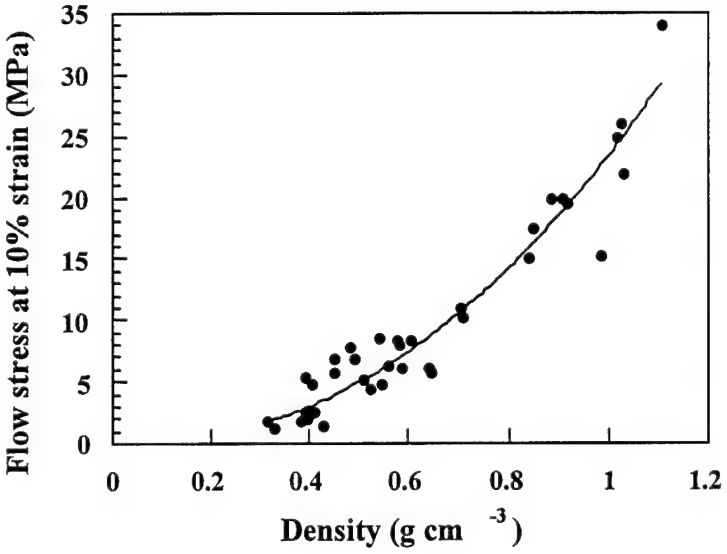

Fig. 10: Flow stress at 10% strain *vs.* density for all samples, independent of strain rate employed.

Microscopic observations

The sequence of deformation events was recorded digitally during quasi-static compression testing. A typical record is presented in Figure 11, as a montage of frames numbered from 1 to 12. The total deformation time from the start of the test until frame 12 was 2 minutes. Frame 1 shows an undeformed region of the foam that contained several cells with the compression loading axis horizontal. As soon as compression starts the thinnest sections of cell walls, approximately parallel to the compression axis, start to buckle, frame 2. In the later stage of deformation, see frames 6 and 9, cell walls normal to the compression axis tear due to the induced tensile strains. It may also be noted that deformation is highly non-homogeneous and localized in the mid-section of the region considered, see frame 12. These types of observations are characteristic of the deformation behavior of the foam in Regions 1 and 2, discussed in Figure 4. As the deformation proceeds, all the cell walls crush and further compression stiffens the foam in Region 3. A typical foam cross-section compressed to 90% strain is shown in Figure 12 representing a substantially densified structure.

Microscopic observation of the interior of cell walls showed clear evidence of the original powder particles; all the walls were made up of many small "bubbles" which were loosely sintered together and many of which exhibited particles on their surface, Figure 13. These bubbles confirmed that melting was incomplete and that the foam was solidified before equilibrium was reached. Many of the particles on the bubble surfaces were identified by X-ray EDS measurements as being rich in Ti.

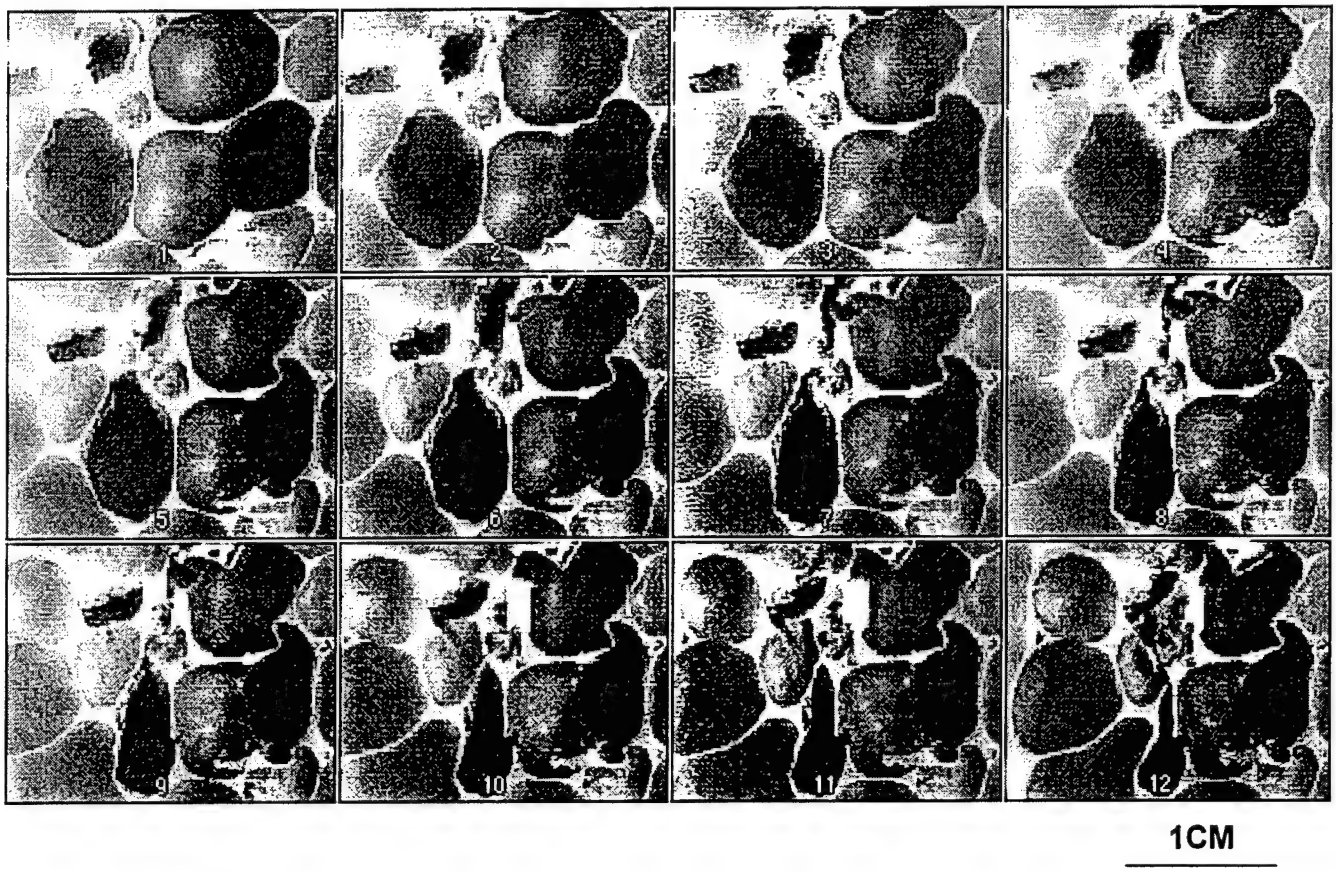

Fig. 11: Sequence of frames during quasi-static crushing of foam sample.

(Compression axis horizontal)

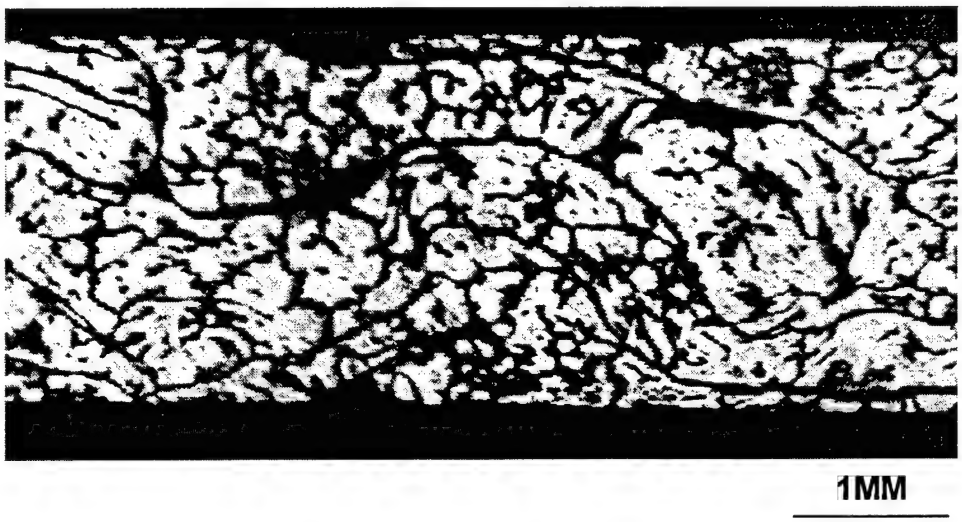

Fig. 12: Foam sample after 85% strain showing extreme densification.

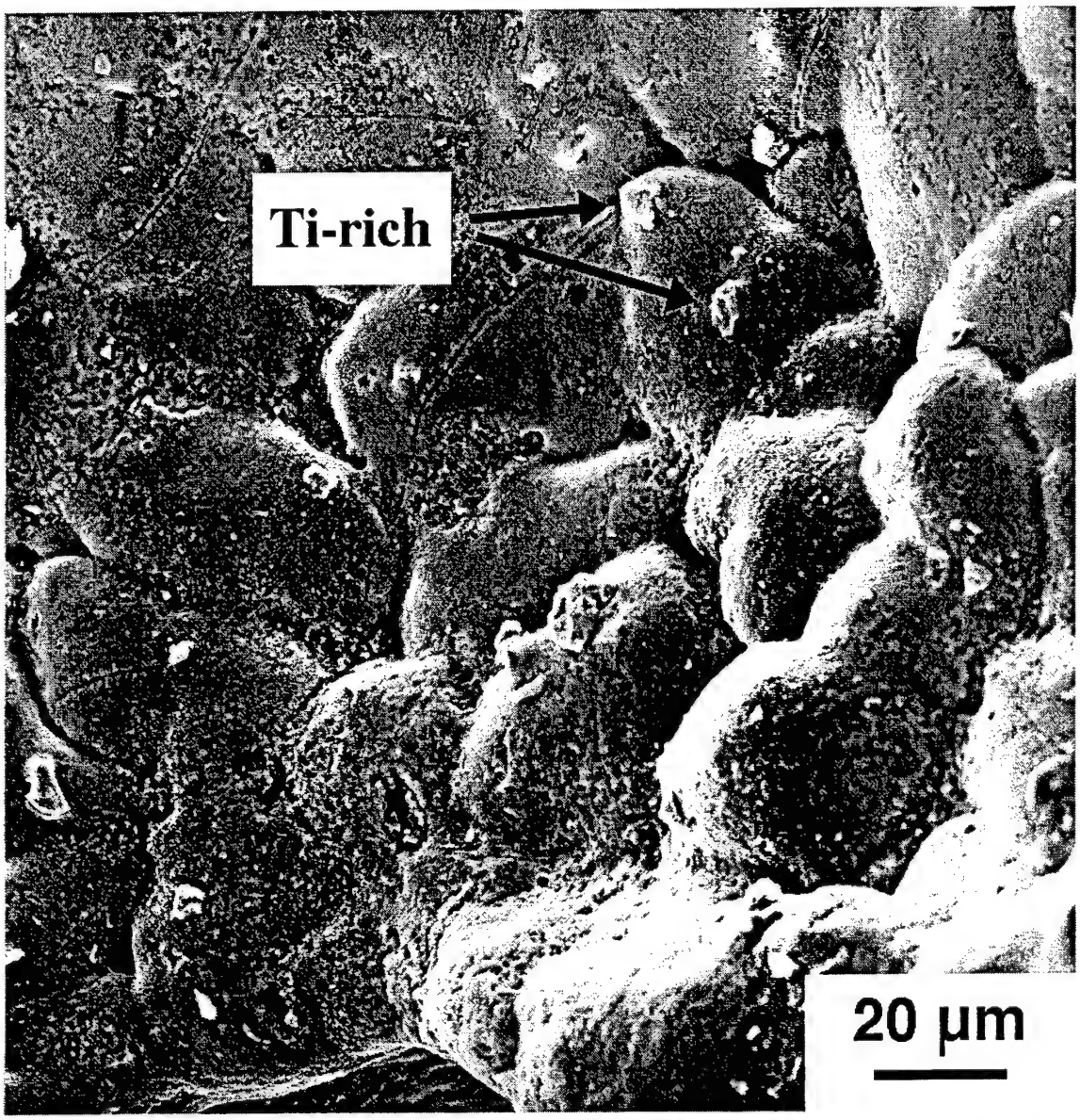

Fig. 13: Interior of pore showing clear evidence of initial Al powder particles, and Ti-rich particles as remnants of the TiH_2 powder.

Discussion

A general expression relating the mechanical properties of open cell foams to their density has been previously proposed [5] as:

$$\frac{X_f}{Xm} = K(\rho^*)^n \qquad \text{Eqn. 3}$$

where X is a property such as the modulus or yield stress, "f" and "m" refer to foam and dense solid metal respectively, and K and n are constants. Equation 3 was developed for open cell foams, while the following equation has been proposed for the yield strength of closed cell foams:

$$\frac{\sigma_f}{\sigma_m} = 0.3\,(\phi\,\rho^*)^{3/2} + (1-\phi)\rho^* \qquad \text{Eqn. 4}$$

where ϕ is a measure of the distribution of solids between cell walls and edges. The first term in Equation 4 is due to bending and the second is due to membrane stretching. It is noted that in both Equations 3 and 4, the foam mechanical properties are proportional to the precursor alloy properties.

In order to determine the effect of strain on the flow stress of the foam, flow stresses were determined at 10% strain and plotted as a function of relative density as shown in Fig. 10. The choice of 10% was somewhat arbitrary but flow stress values at small strains, such as the yield strain, can not be used for comparison purposes due to lack of stress equilibrium in the early stages of the test; this is an inherent feature of the SHPB apparatus. Quasi-static and dynamic flow stresses were fitted to the power law equation (Eqn. 2 on page 16). It was found that Eqn. 2 fits all the flow stresses quite well for both quasi-static and dynamic cases, although the value of the exponent n was found to be higher than the previously reported values of approximately 1.5.

No effort has been made here to separate the data on the basis of strain rate and it is recognized that this simple fit may hide a multitude of independent density/strain rate/flow stress/strain rate sensitivity relationships. Future work will certainly address the issues of determining these complex inter-relationships.

Ballistic testing and stress wave measurements in penetrated targets

Figure 14 shows diagrams of the first two targets that were used to measure the effect of aluminum foam layers on impact stress waves. The stress wave targets were designed to maximize the effects of impact induced stress waves in order to increase the chance of detecting a shock or stress absorbing effect of the metal foam. The stress wave targets were not designed to resist penetration of the projectile. The benchmark stress wave target (target without the metal foam) was designed to maximize the deleterious effects of impact induced stress waves on a ceramic element. In an armor design utilizing a metal cover plate over the ceramic tile, stress waves from impact of the projectile on the metal cover plate can run ahead into the ceramic and failure may initiate prior to the projectile even contacting the ceramic tile; thus, a steel impact plate was used in these targets. The amplitude and frequency of the stress waves produced at impact vary greatly with the nose shape of the projectiles, e.g. ogive vs. cylindrical. The highest amplitude waves have been measured for impacts with Fragment Simulating Projectiles (FSP). Thus the 20-mm FSP was chosen to maximize the stresses. Figure 15 shows the dimensions of the FSP projectile per MIL-P-465934A. The aluminum back plate was primarily used to facilitate mounting of the targets in the target fixture. In the second target design with a metal foam layer, the foam layer was expected to absorb shock energy from the projectile impact and thus delay damage in the ceramic layers and improve their performance.

The layers of the targets were bonded together with a thin layer of fast setting epoxy adhesive. The stress gage was also encased in two 0.18-mm thick Kapton polyamide plastic sheets. Both targets had a similar areal density. The one without a foam layer had an areal

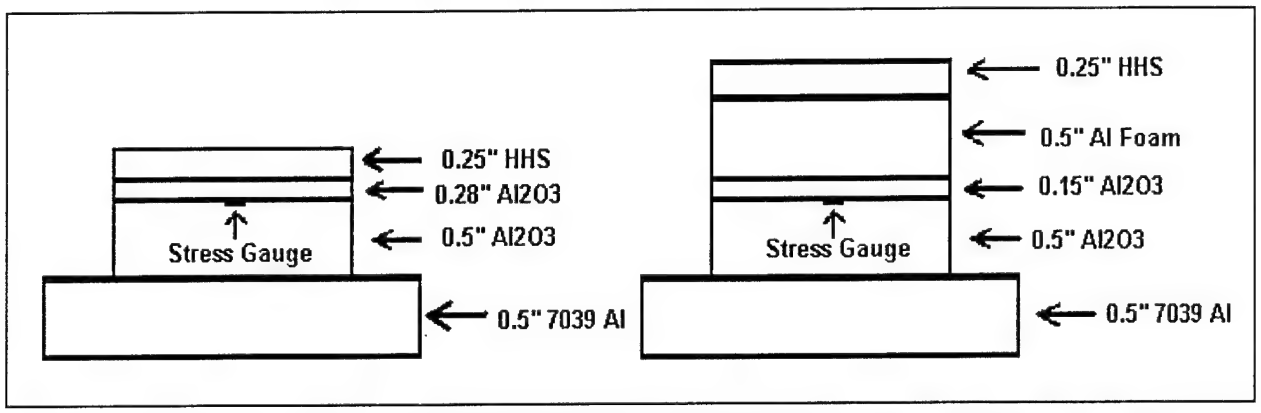

Figure 14: Target design without strike plate; two tests were conducted with and without aluminum foams.

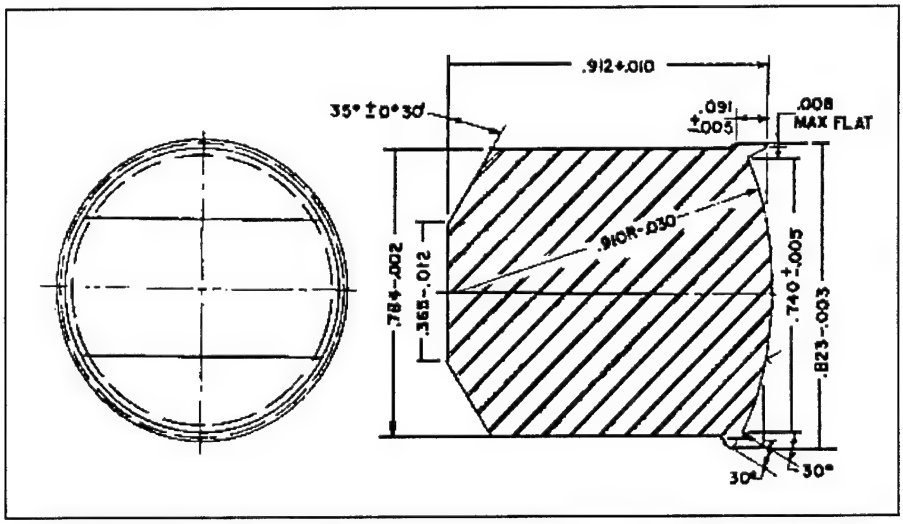

Figure 15: Dimensions of the 20-mm Fragment Simulation Projectile.

density of 32.98 psf (pounds per square foot) and the one with a foam layer had an areal density of 32.31 psf. The 20-mm FSP threat projectile was fired at 1,067 m/s (3,500 fps) for these ballistic experiments.

Figure 16 shows the stress wave profiles measured in the experiments. The stress profile in the experiment without the metal foam has a rise time of approximately 1 μs. The oscillations occur on a time scale that is too short to allow free surface reflections. The smaller oscillations in the rise of this signal are probably due to (so called) "ringing up" of the stress wave as it

reflects back and forth through the thickness of the gage and its protective plastic films and reaches the stress in surrounding ceramic materials.

The arrival time measured in the first experiment, without Al foam, is 15.335 μs. The calculated arrival time is 14.6 μs, less than 1 μs different than the measured value. The estimate arrival time was calculated using approximate bulk wave speeds, 3.5 km/sec for steel and 7.5 km/sec for alumina, an offset trigger distance of 0.5", and a projectile speed of 1.067 km/sec. Errors in these approximate wave speeds combined with experimental uncertainties, such as electronic rise times, account for the difference between the calculated and measured values. The substantial agreement between the calculated and measured arrival time indicates that the wave profile is for the impact induced stress wave.

The stress wave measured in the second experiment, with Al foam, has a surprisingly high amplitude. Aluminum has only about half the acoustic impedance of either steel or the alumina ceramic, thus only about half the amplitude of the stress wave impinging the aluminum foam should be transmitted to the ceramic and subsequently the gage. Rise time of the stress wave is larger than the rise time measured in the first experiment, as is expected for a wave travelling through such a heterogeneous porous structure as is present in the foam. Also, the arrival time is not surprising. Assuming a wave velocity through the aluminum foam of 1 km/sec results in a calculated arrival time of 27.3 μs, versus the measured value of 29.95 μs. Based on a rule of mixtures, an aluminum material with 80% porosity should have an acoustic wave velocity approximately 20% of fully dense aluminum. The bulk wave speed in fully dense aluminum is 5.35 km/sec, thus 1 km/sec is a reasonable approximation for the bulk wave speed through the foam. Unfortunately, this arrival time is also consistent with the time at which the projectile itself is calculated to reach the aluminum oxide face. Considering these observations, a reasonable explanation that accounts for the observed arrival time, small amplitude toe, overall rise time, and final high amplitude, is:

- the initial signal is caused by arrival of the stress wave produced when the projectile impacted the target face (the steel),
- this wave rises to a very small amplitude, less than ½ GPa,
- approximately ½ μs later the projectile crashes into the aluminum oxide face producing the high amplitude wave.

Further experiments should be conducted to verify this explanation. If this is true, then the aluminum foam effectively dissipated the impact-induced stress wave, protecting the aluminum oxide from premature failure that may have occurred from transit of this wave into the ceramic. Post test observations of the targets show that the target with the foam layer performed marginally better at a slightly lower areal density.

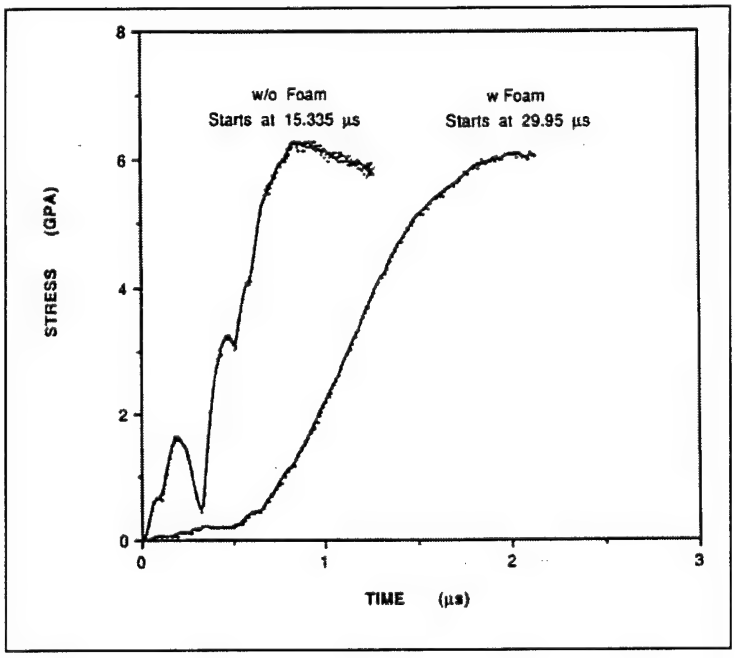

Figure 16: Recorded stress signals after ballistic impact (with and without Al foam insert).

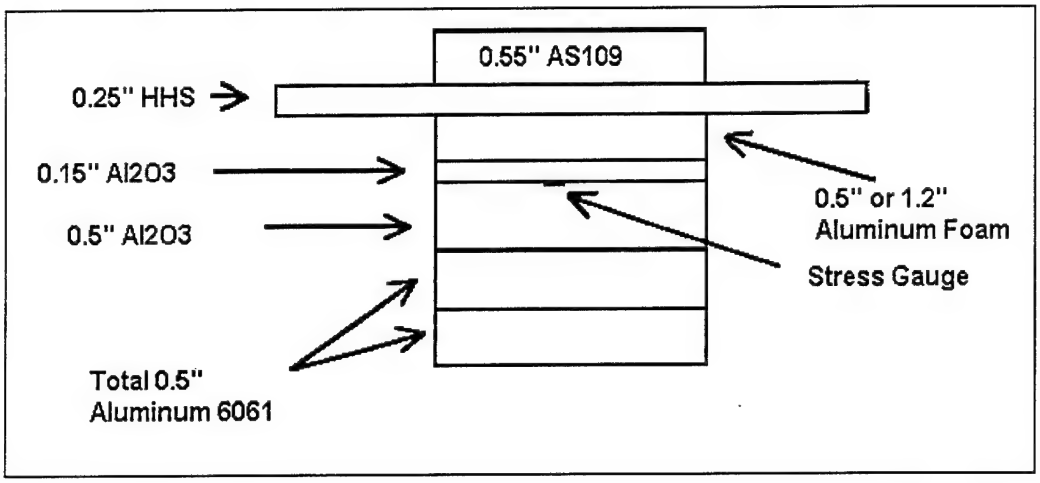

Figure 17: Target design with the AS109 ceramic matrix composite strike plate; two tests were conducted with 0.5" and 1.2" thick aluminum foam insert.

Stress wave measurements behind non-penetrated targets

Figure 17 shows schematic diagrams of the two targets used in these experiments. This target arrangement was selected to facilitate stress wave measurement, not for its ballistic efficiency. Backface-effect targets were designed to provide a preliminary assessment of the aluminum foam's ability to absorb stresses and deformation energy in a way that protects fragile components located behind the target. This approach was followed after considering real armor effects in which the armor resists penetration by the projectile, but backface responses of the armor damages or destroys the very personnel or equipment that the armor is intended to protect. The first two layers consisted of a hexagonal shaped DIMOX-AS109 impact tile and a steel plate, simulating the armor that was intended to arrest the penetrator. AS109 is a ceramic matrix composite produced by Lanxide Armor Products with particulate SiC in an Al2O3 matrix with a small amount of aluminum. It has a density of 3.3 gcm^{-3}. The Al2O3 ceramic tile behind this armor simulant is intended to simulate a "fragile component" that may be harmed by backface responses of the armor. Stresses transmitted into the ceramic were measured with the manganin/constantan gage. The aluminum plates behind the ceramic plates were utilized to support the ceramic and enable post test recovery. Metal foam layers were located between the steel plate of the "armor simulant" and the ceramic "fragile component" in order to protect the

fragile component. The 20 mm FSP was fired at 915 m/s (3000 fps) velocity to preclude penetration of the AS109 /High Hardness Steel base target in front of the aluminum foam layers.

Figures 18-21 show the individual target layers after the ballistic impact. The AS109 strike face was shattered upon the ballistic impact (Figure 18). The High Hard Steel plate was deformed but not penetrated (Figure 19). Deformation of the High Hard Steel plate was significant enough that the deformation energy penetrated through the 0.5" thick aluminum foam plate and shattered the Al2O3 back plate (Figures 20-21). Figure 22 shows the stress profile measured in the Al2O3 ceramic with the 0.5" thick aluminum foam layer behind the base target. The signal has a rise time of over 20 microseconds and starts 35.3 microseconds after impact. The original impact stress wave should have traveled through the AS109 and High Hardness Steel layers in only about 3 microseconds. Thus, the measured stress wave either took a very long time to traverse the foam (32 microseconds, corresponding to a wave velocity of 0.4 km/sec) or, more likely, was produced by the deformation of the steel backplate through the foam and into the Al2O3.

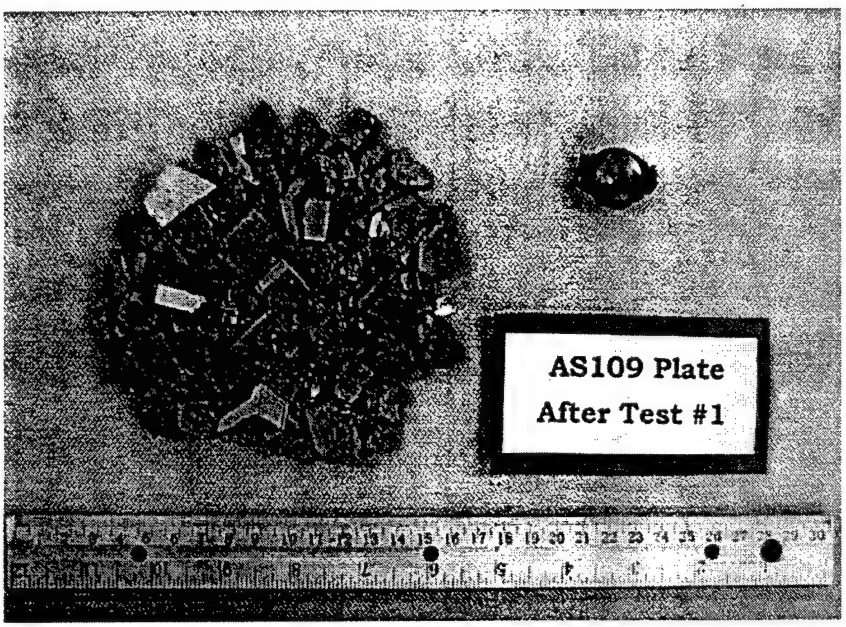

Figure 18: AS 109 Plate after the ballistic testing.

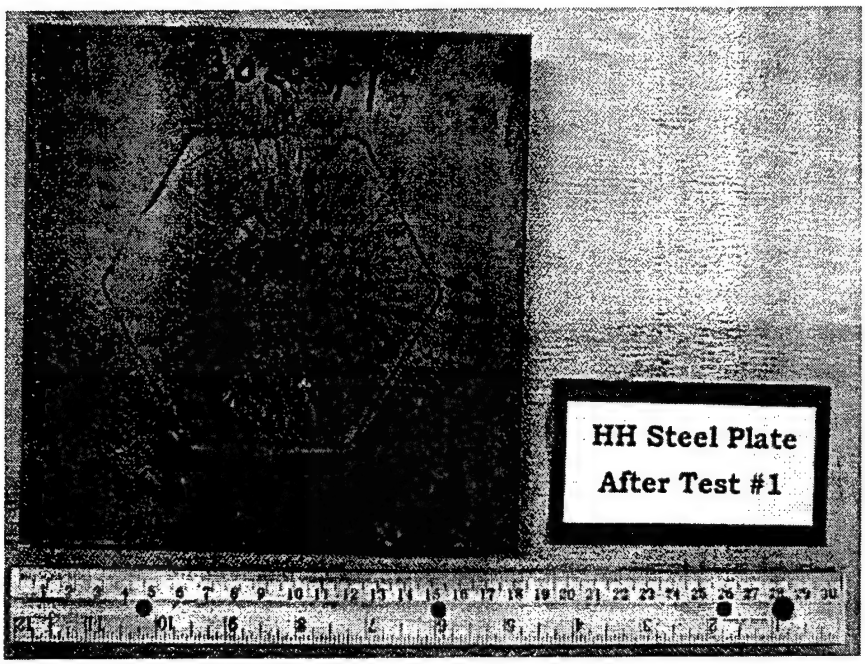

Figure 19: High hard steel after ballistic testing.

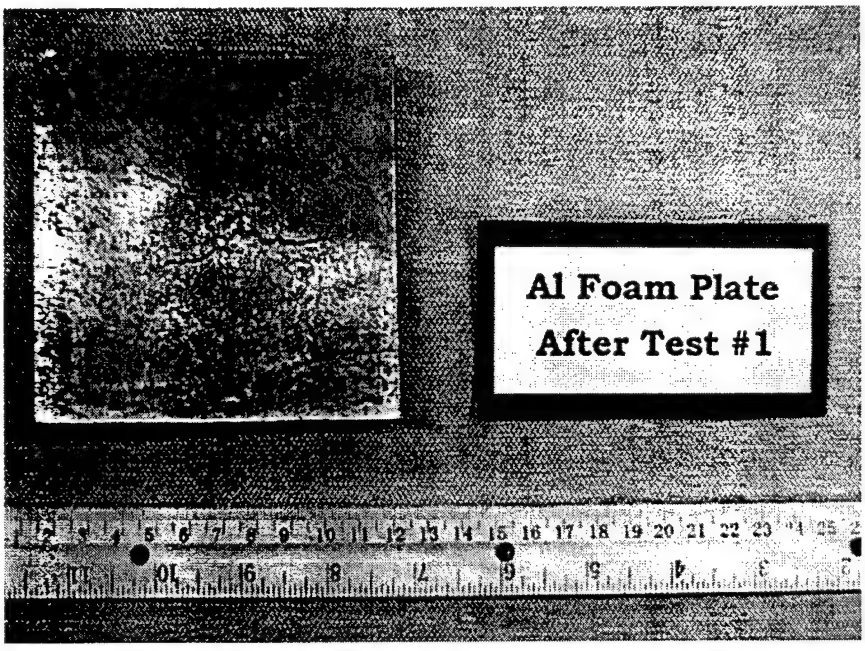

Figure 20: 0.5" aluminum foam after ballistic testing.

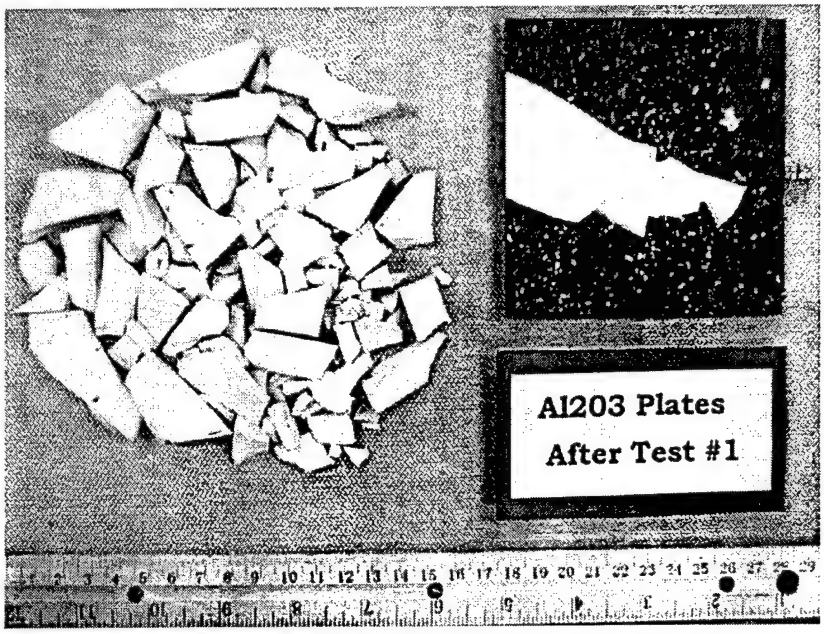

Figure 21: Al2O3 backing plate after ballistic testing.

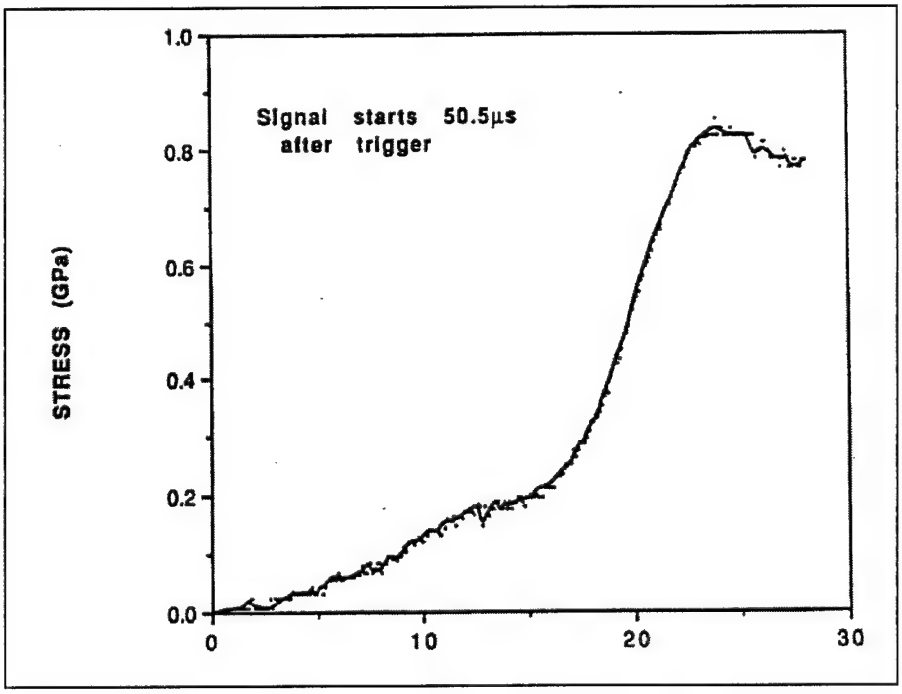

Figure 22: Recorded stress signal after ballistic testing (with 0.5" thick foam insert).

FSP ballistic testing was also conducted on the same target arrangement, as shown in Figure 17, but with a 1.2" thick aluminum foam insert. Figure 23 shows the deformed aluminum foam plate and Figure 24 is the unbroken Al2O3 back plate after impact. No measurable stress wave was observed with the 1.2" thick aluminum foam layer behind the base target.

Postmortem examination of the two targets showed that the 0.5" thick aluminum foam layer was deformed through its thickness by the bulging steel back plate and the Al2O3 ceramic layer were fractured into small pieces. In the other experiment the 1.2" foam layer completely contained the bulge and protected the Al2O3 ceramic from damage. It contained only small cracks that may have formed during recovery of the target components after testing.

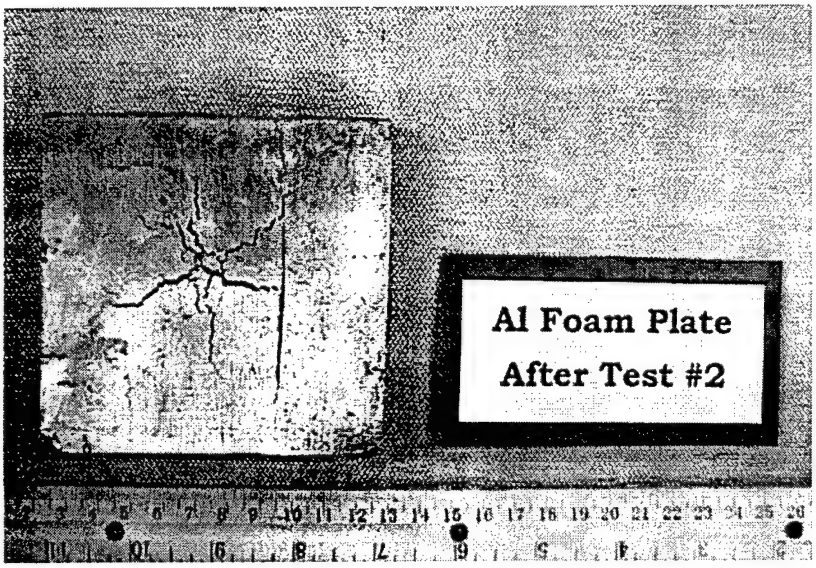

Figure 23: 1.2" thick aluminum foam plate after ballistic testing.

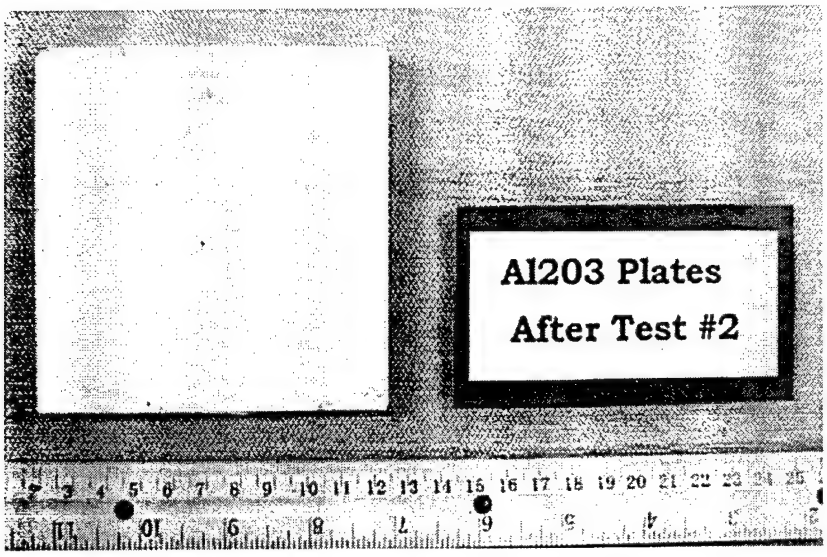

Figure 24: Al2O3 plate after ballistic testing.

The 1.2" thick aluminum foam insert after the FSP testing was cross-sectioned by EDM (Electro-Discharge Machining) to reveal the deformed microstructure. Figure 25 shows the representative microstructure indicating the deformation sequences of the cell structure. It is suggested that the deformation energy first densified the upper portion of the aluminum foam. Subsequent deformation introduced tearing and shearing of the cell walls, as illustrated earlier in Figures 11 and 12, an effect of core shearing deformation for energy dissipation. In this case, the deformation energy was redirected and dissipated sideways. Similar deformation mechanisms can also be observed at low strain rates.

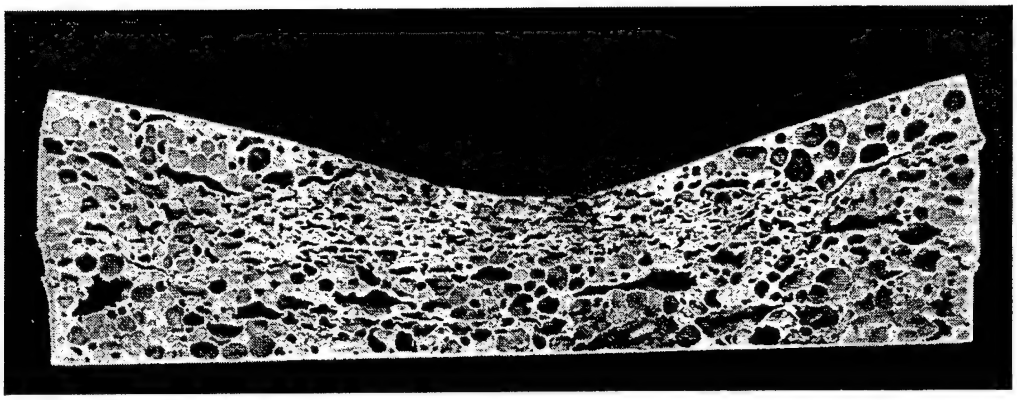

Figure 25: Cross-sectioned microstructure showing the deformation sequences.

5. SUMMARY AND CONCLUSIONS

The deformation energy absorption capability of aluminum 6061 foam was evaluated with a range of strain rates up to the ballistic ranges. The following can be concluded based on the test results:

- The results from the quasi-static compression tests and the SHPB tests show that the compressive flow stress of the aluminum foam was a function of the relative density. Also, the flow stress is essentially independent from the strain rate.

- Compression deformation of the foam was in the form of cell wall buckling and tearing, which occurred locally then, progressed throughout the sample. Finally, foam was densified due to cell wall touching.

- The results from the preliminary ballistic stress wave experiments show that the metal foam in front of the ceramic element has a strong effect on the shape and arrival time of the stress waves in the aluminum oxide ceramic, and may be effectively protecting the ceramic from premature failure.

- The "behind-the-target" measurements show that the metal foam is effective in containing rearward deformation of a ballistic target, and may thus be useful for controlling backface deformation and spalling and thereby provide added protection to equipment and personnel.

6. SUGGESTIONS FOR FUTURE WORK

Based on the results obtained to date, the following are suggestions for future work to be conducted:

Fabrication of aluminum foams

- Maximization of energy absorption by adjustment of foam parameters such as cell size, wall thickness, and uniformity. Metal foams with different alloying elements and density levels can be fabricated for further evaluation.
- Investigation of alternate foamable alloys, and effects of heat treatments upon energy absorption.
- Effect of modulus improvement due to addition of particulate or whisker reinforcements to metal foams.

Split Hopkinson Pressure Bar testing

- Modification of SHPB apparatus and data reduction to permit more accurate data generation from low impedance foams.
- Further study on deformation mechanisms of aluminum foams as a function of strain rate.

Ballistic and blast protection:

- Effects of stress wave management via metal foam on ballistic or blast efficiency, and the placement of metal foam for maximizing efficiency of ballistic (including other types of ballistic testing) and blast protection.
- Utilization of aluminum foam to reduce backface deformation without sacrificing ballistic efficiency behind targets with highly deforming backplates.
- Utilization of metal foams for spall suppression behind titanium, aluminum, steel or other armors prone to spalling.
- Computer simulation of the deformation sequences on the target with metal foam inserts.

7. REFERENCES

(1) M.F. Ashby, "The Mechanical Properties of Cellular Solids", Metall. Trans. Vol. A14, 1983, pp.1755-1769.

(2) J. Baumeister and H. Schrader, "Method for Manufacturing Foamable Metal Bodies", U.S. Patent No. 5,151,246.

(3) G. T. Gray III, Methods in Materials Research, (Wiley, New York, NY) 1997.

(4) R.E. Franz and W. Lawrence, "Stress Measurements in Glass During Shaped-Charge Jet Penetration", U.S. Army Ballistic Research Laboratory Memorandum Report BRL-MR-3518 (1986).

(5) L. Gibson, M.F. Ashby, Cellular Solids, Oxford University Press, Oxford (1997)

8. Bibliography

This work was coordinated by Dr. Chin-Jye (Mike) Yu, Program Manager for Ultralight Weight Materials at FRC-DE, and Dr. Harald Eifert, Executive Director of FRC-DE, in close collaboration with Professor Ian W. (Rick) Hall of UD, and Mr. Robert E. Franz of Lanxide Armor Products Inc. The following is a short list of biographical information:

Fraunhofer Resource Center - Delaware

Dr. Chin-Jye (Mike) Yu

Education

Ph.D. Engineering Science and Mechanics 1991
The Pennsylvania State University

Professional Experience

Fraunhofer Resource Center - Delaware
Program Manager, Ultralight Weight Materials Since 08/1998
Program Manager, Metal Foams 1997-1998
Concurrent Technologies Corporation, Johnstown, PA
Senior Mechanical Engineer 1996-1997
Engineer 1991-1996

Selected Publications

- Metal Foaming by a Powder Metallurgy Method: Production, Properties and Applications, Journal of Materials Research innovations (1998)

- Investigation for the Selection of Foaming Agents to Produce Steel Foams, Proc. of the 1998 MRS Symposium on Porous and Cellular Materials for Structural Applications (1998)

- A Semi-Empirical Model for the Elastic Properties of P/M Steel Alloys as a Function of Density, Proc. of the 1994 P/M Congress (1994)

- Determination of Dynamic Elastic Properties in Powder Metallurgy Components - An Evaluation from an Industrial Standards Program Perspective, Review of QNDE (1992)

Fraunhofer Resource Center - Delaware

Dr. Harald H. Eifert

Education

Doctor Engineer, Mechanical Engineering — 1994
Technische Universität Clausthal, Germany, Fakultät für Bergbau, Hüttenwesen und Maschinenwesen

Professional Experience

Fraunhofer Resource Center - Delaware
Executive Director — Since 07/1998
Technical Director — 1996-1998
Fraunhofer Institute for Applied Materials Research, Bremen, Germany
Head of Project Group Powder Metallurgical Forming — 1994-1996
Project Manager, Nanopowder Technology — 1989-1994

Selected Publications

- A Case Study for a Complex Shaped Part Made by Powder Injection Molding of Tungsten Heavy Alloy, Proc. of the International Conference on Tungsten and Refractory Metals and Alloys (1997)

- CVR Production and Sinter Characteristics of Tantalum Nanopowders, Proc. of the International Conference on Tungsten and Refractory Metals and Alloys (1997)

- Powder Injection Molding of the intermetallic Phases Ni-Aluminides and Silizides, Proc. of the second International Symposium on Intermetallic Phases (1997)

- Rapid Prototyping of Functional Metal and Ceramic Components by the Multiphase Jet Solidification (MJS) Process, Proc. of the 1997 Solid Freeform Fabrication Conference (1997)

- Binder Design and Process Control for High Performance MIM-Materials, Proc. of the 1995 P/M Congress (1995)

University of Delaware

Dr. Ian W. Hall

Education

Ph.D. Metallurgy University of Leeds, U.K.	1974

Professional Experience

University of Delaware	
Chairperson, Materials Science Program	1989-1996
Associate Professor, Dept. of Mechanical Engineering	Since 1987
Assistant Professor, Dept. of Mechanical Engineering	1982-1987
Visiting Assistant Professor, Dept. of Mechanical Engineering	1980-1982
Technion, Haifa, Israel	
Lady Davis Research Fellow, Dept. of Materials Engineering	1978-1980
Technical University of Denmark	
Lecturer, Dept. of Metallurgy	1975-1978

Selected Publications

- "Quasi-static and Dynamic Compression Behavior of an FP™ Alumina Reinforced Aluminum Metal Matrix Composite", M. Guden and I. W. Hall, J. Mat. Sci., 33 (1998) 3285

- "Dynamic Properties of Metal Matrix Composites: A Comparative Study", with M. Guden, Matls. Sci. & Eng.A, A242 (1998) 141

- "High Strain Rate Behavior of an SiC Particulate Reinforced Al_2O_3 Ceramic Composite", with M. Guden, Scripta Materialia, 38, (1998) 667

- "High Strain-Rate Compression Testing of a Short-Fiber Reinforced Aluminum Composite", with M. Guden, Matls. Sci. and Eng. A, A232, (1997) 1.

- "Dynamic Compressive Behavior of a SiC_w/Al Composite", with A. Kalambur, Scripta Materialia, 37, 1997, p. 193

Lanxide Armor Products Inc.

Mr. Robert E. Franz

Education

M.S. Electrical Engineering — 1952
University of Wisconsin

Professional Experience

Lanxide Armor Products Inc.
Application Engineer, Armor System — Since 1987

Army Ballistic Research Laboratory
Team Leader, Solid Mechanics Branch, Terminal Ballistics Division — 1953-1987

Relevant Experience

- Principal designer for lightweight hatch technology demonstration for Bradley Vehicle
- Development and design for top armor for the defeat of fragment threats on the Composite Armor Vehicle (CAV) of General Dynamics Land System
- Design ballistic solution for the ALCOA Propulsion Systems Demonstrator (PSD) using Lanxide ceramic matrix composites and Kevlar reinforced plastics
- Target design using Lanxide ceramic matrix composite for protection against 0.5 cal AP-M2 and 0.5 cal 20 mm FSPs for Naval Surface Warfare Center